Towards A Predictive Model of the Shear Strength Behaviour of Fibre Reinforced Clay

Author 1*

Jianye Wang ORCID: 0000-0001-5889-1414

Affiliation: Lecture in School of Civil and Transportation Engineering, Beijing University of Civil Engineering and Architecture, China.

Author 2

Paul N Hughes ORCID: 0000-0002-7260-794X paul.hughes2@durham.ac.uk

Affiliation: Associate Professor in the Department of Engineering, Durham University, Durham, UK.

Author 3

Charles E Augarde ORCID: 0000-0002-5576-7853 charles.augarde@durham.ac.uk

Affiliation: Professor in the Department of Engineering, Durham University, Durham, UK.

***Corresponding author: Jianye Wang**

Email Address: wangjianye@bucea.edu.cn

Number of words in the main text: 6554 (without captions and references)

Number of figures: 15

Number of tables: 4

Abstract: Randomly distributed fibres can be a potential reinforcement material to improve the shear strength of soils. However, gaps remain in experimental research and predictive modelling of the shear strength of fibre reinforced high plasticity clays. In light of this, a series of consolidated undrained triaxial tests were carried out to investigate the shear strength behaviour of London Clay reinforced with 0.3% to 0.9% polypropylene fibre by dry weight of soil. The effects of fibre length and confining pressure were also considered. The results indicated that fibres significantly improve the shear strength of soil. The shear strength improvement increases with the fibre length, but decreases with increasing confining pressure at test scale. The addition of fibres also leads to the increase in the pore water pressure of soil. Using these and other experimental results, a predictive model was developed based on the concept of equivalent confining stress. The model is able to describe the deviator stress-strain and pore water pressure-strain relationship of fibre reinforced clay and can be used efficiently to predict the shear strength of fibre reinforced clay subjected to different confining pressures.

Keywords: fibre reinforcement; high plasticity clay; shear strength; predictive model

1. Introduction

The need to expand and develop infrastructure in response to population growth and economic development frequently requires construction works in areas of problematic soils. Locally available cohesive soils, especially high plasticity clay, are often used as backfill materials to produce earthen structures, e.g. highway embankments and flood defences (Gunn et al. 2015). However, some of these soils cannot meet the strength requirements of earthworks construction without additional strengthening, often referred to as "stabilisation" and the failure of earthen structures is often linked to poor engineering properties of high plasticity clays, cases being found all over the world (Briggs 2010; El Mountassir et al. 2011; Khan et al. 2017).

High plasticity clays also have a high potential for volume change when exposed to cycles of rainfall and drought and of cracking resulting in water infiltration, and a reduction in shear strength. An increase in the number of periods of extreme heat and intense precipitation in the coming decades as a result of climate change is likely to result in additional damage and loss of stability to earthen infrastructure in many parts of the world (IPCC, 2014; Tang et al., 2018).

For many years, problematic soils have been improved by a range of ground improvement methods including soil mixing with chemical or bio binders (Consoli et al. 2018; Yu et al. 2020; Ni et al., 2020; Ni et al., 2022). In recent decades, the use of randomly distributed fibres as a soil stabilisation material has attracted increasing attention due to its ease of use, low cost and since it can provide isotropic reinforcement. In the academic field, a number of experimental and analytical investigations have been conducted into the mechanical properties, especially shear strength, of fibre reinforced soil.

In laboratory studies, direct shear tests (Mirzababaei et al. 2017; Hazirbaba et al. 2018; Aouali et al. 2019; Han et al. 2020) and triaxial tests (Mandolini et al. 2019; Patel and Singh 2019; Foresta et al. 2020; Karimzadeh et al. 2021) have demonstrated that shear strengths of sandy and low plasticity cohesive soils are increased when reinforced with various types of fibres. However, fewer studies can be found on fibre reinforced high plasticity clay (Akbulut et al. 2007; Kalhan 2013; Mirzababaei et al. 2018; Ekinci 2016; Taha et al. 2020; Correia et al. 2021). Despite the conclusions drawn by these studies that fibres can improve the shear strength of high plasticity clay generally, consensus has not been reached on the following points.

- On the effects of fibre inclusion ratio, i.e. the ratio of mass of fibres to mass of dry soil (see Equation (1) below), Kalkan (2013) and Taha et al. (2020) conducted direct shear tests on high plasticity clay reinforced with rubber and polypropylene fibres respectively and drew different conclusions. The friction angle of soil in the former study increased as the fibre inclusion ratio increased from 0 to 2%, then decreased with further addition of fibre. In the latter study, the friction angle of soil increased as the fibre inclusion increased from 0 to 3%.
- As for the influence of fibre length, Mirzababaei et al. (2018) conducted a series of reverse drained direct shear tests on fibre reinforced high plasticity clay and reported that the cohesion of the soil increased then decreased as the fibre length changed from 6 to 19 mm. However, in direct shear tests conducted by Akbulut et al. (2007), it was found that the change in cohesion of the high plasticity clay used there had no obvious relationship with the fibre length.

- On the influence of confining pressure, Correia et al. (2021) and Ekinci (2016) conducted a series of triaxial undrained (CU) and drained (CD) tests on polypropylene (PP) fibre reinforced clay. In Correia et al. (2021), a reduction in improvement of shear strength was observed with increasing confining stress from 50 to 300 kPa. In Ekinci (2016), a threshold value of confining pressure (150 kPa) was found. Fibre reinforced soils (FRS) show higher shear strength than equivalent unreinforced soils (URS) when the confining pressure is lower than this value; unreinforced samples show greater strength when the confining stress higher than this value.

When it comes to analytical investigations, most predictive models of fibre reinforced soil have focused on granular materials (Gray and Ohashi 1983; Michalowski and Zhao 1996; Zornberg, 2002; Michalowski and Cermark 2003; Chen 2007; Diambra et al. 2010; Gao and Zhao 2012; Ajayi et al. 2016; Gao and Diambra 2020). As for cohesive soils, Diambra and Ibraim (2014) proposed a constitutive model for fibre reinforced clay by superimposing the stress contribution of elasto-plastic fibres within a modified Cam Clay model. The slippage and pull-out of the fibres and the breakage of the fibres were taken into account in this model and six parameters were introduced to describe the fibre stress-strain response and fibre-soil interaction mechanisms.

Jamei et al. (2013) derived a model that enables prediction of the failure of fibre reinforced clay based on the energy homogenization scheme proposed by Michalowski and Zhao (1996), in which the behaviour of a specific fibre-clay interface is taken into account as part of the failure mechanism of the FRS. Two parameters (cohesion and friction angle of the interface) which are obtained from pull-out tests of fibres are introduced. Wang et al. (2018) developed a predictive model for pre-failure and failure behaviours of fibre-reinforced clay by combining the superposition method (Diambra and Ibraim 2014) and an energy based homogenization technique (Jamei et al. 2013). The relationship between the stiffnesses of the clay and fibre phases is built via the strains of fibres and soil, and the pre-failure and failure behaviour of fibre reinforced clay is described by the composite's stiffness matrix and fibre's stiffness matrix respectively.

A review of the literature suggests that more laboratory investigations are required into the effects of fibre inclusion ratio, fibre length and confining pressure on the shear strength behaviour of fibre reinforced high plasticity clay. Existing models of fibre reinforced clay are mostly based on complex calculations and the parameters necessary to run these models need a series of extra tests on materials. A practical model for predicting the shear strength of fibre reinforced clay is necessary. To this end, in this study, the effects of polypropylene fibre reinforcement on the shear strength behaviour of London Clay are investigated via a series of CU tests. The influences of fibre length and confining pressure are taken into account. Based on the test results, a practical model is proposed in order to predict the stress-strain and pore water pressure-strain relationships of fibre reinforced clay with less experimental and analytical efforts.

2. Materials and methods

London Clay was obtained from an excavation site for Crossrail in Clapham, London, UK. Classification and compaction properties of the soil were determined in accordance with BS 1377-2 (BSI, 1990), and are shown in Table 1. The basic properties of the polypropylene (PP) fibre used this study are given in Table 2, and the appearance of the fibre is shown in Figure 1.

To prepare the soil-fibre composite, designated masses of fibres were firstly mixed manually with air dried soils, followed by distilled water. This mixing method resulted in less fibre lump formation because fibres are first coated by a layer of dry clay and then mixed well with water (Mirzababaei et al., 2012). The wet composite was then further mixed by a laboratory mixing machine for 3 minutes until a homogeneous mix was achieved. The details of the whole process can be found in Wang (2020). The triaxial samples were then statically compacted in a 38 mm diameter × 76 mm high cylindrical mould in three equal layers. All the samples were compacted at each soil's optimum water content and maximum dry density (MDD), as determined by standard Proctor compaction tests to BS 1377-4 (BSI, 1990). The MDD was selected as each sample's initial dry density (ρ_d) to represent field conditions.

Consolidated undrained triaxial tests were then conducted in accordance with BS 1377-8 (BSI, 1990). The specimen was back pressure saturated at 300 kPa and with 5 kPa difference between cell pressure and back pressure, ensuring B values of at least 0.95 for each specimen. Then the specimens were isotropically consolidated at a predefined confining stress until there was no volume change. After consolidation, specimens were sheared at an axial strain rate of 0.02% per minute, until a serviceability failure criterion of 20% axial strain. Three different fibre inclusion ratios (ρ_f = 0.3, 0.6 and 0.9% as shown in Equation 1) and two different fibre lengths (l_f = 6 and 12 mm) were used in tests.

（1） $\rho_f = \frac{m_f}{m_s} = \frac{W_f}{W_s}.$

where m_f and m_s are the masses of fibre and dry soil respectively, W_f and W_s are the weights of the fibres and dry soil respectively (to be used in the model derivation later). The confining pressures applied in this study were 50, 100 and 200 kPa, selected to simulate the condition of soils in embankment engineering. The characteristics of the specimens are shown in Table 3, in which unreinforced soil and reinforced soil are represented by URS and FRS respectively, A to C and D to F represent fibre inclusion ratio from 0.3 to 0.9% for two different fibre lengths, numeric suffixes represent different reinforcement conditions and confining pressures.

It is worth mentioning that an extra test was conducted on an unreinforced sample having original dry density 1.581Mg/m^3 with the same water content as the 6 mm 0.9% FRS sample (w=21.3%), the test results (Wang, 2020) showing that this tested sample had a similar response to that of the original URS sample. This extra test was undertaken to eliminate the potential difference of shear strength increment from slightly initial different water contents.

3. Triaxial test results of unreinforced and fibre reinforced soil

The triaxial test results are discussed in several different ways in this section. As a measure of shear strength, the deviator stresses of specimens at serviceability failure (q_f) are shown in Table 3.

Effect of fibre inclusion ratio on the deviator stress

Figure 2 shows the variations of deviator stress (q) with axial strain (ε_1) for the unreinforced and selected fibre reinforced soils. It can be seen from Figure 2 that the deviator stress of soils at the serviceability failure state of 20% axial strain (Diambra et al., 2010) increases with fibre inclusion ratio. This is because a higher quantity of fibre will lead to higher interfacial friction between the fibre and soil, thus increasing the shear resistance of the soil. Also, for the URS specimens, the deviator stress increases sharply during the initial stages of the test, then becomes steady until serviceability failure. For the FRS specimens, however, no peak values can be observed in the plots. It can be concluded that greater fibre inclusion increases the degree of hardening response comparing with the unreinforced sample. Before shearing, fibres in the composite are either bending or stretching due to compaction during sample preparation. Consequently, tensile resistance is only mobilised in the fibres after the sample has undergone some straining, and develops until the majority of the fibres break or pull out. The strength improvement at large strain suggests the potential application of fibre reinforcement in constructions which suffer excessive deformation like embankments over soft soils.

To make comparisons, for a given strain level, we define deviator stress increment (Δq) as

$$\Delta q = q_r - q_u \quad (2)$$

where q_r and q_u are the deviator stresses of the FRS and URS specimens under the same test condition at that strain level, respectively. Figure 3 shows the relationship between axial strain and Δq for different FRS specimens. In general, Δq increases as the axial strain increases and the rate of increase reduces as the axial strain increases further. The decrease in growth rate might come from increased relative sliding between soil particles and fibres. Also, the rate of shear strength improvement reduces with increasing fibre inclusion ratio. For example, when fibre inclusion ratio doubles from 0.3% to 0.6%, the deviator stress increment at serviceability failure only increases by 28% from 24.4 kPa to 31.2 kPa.

Effect of fibre length on the deviator stress

Figure 2b shows that the deviator stresses at failure of FRS specimens also increases with the fibre length. Compared with specimens at 200 kPa confining pressure, specimens at 100 kPa show a more significant difference in deviator stress when reinforced with different fibre lengths, so the effect of fibre length on deviator stress might be influenced by confining pressure level, which need to be proved by more tests. It is known that the friction between soil particles and fibres is mobilised along the length of the fibre, hence longer fibres will increase the overall pull out resistance. In studies (Mirzababaei et al. 2017; Han et al. 2020) including direct shear tests of fibre reinforced soil, optimum fibre lengths were found to be 10 and 9 mm respectively, beyond which the increasing fibre length had a negative influence on shear strength improvement. This value was approximately 20 mm in other triaxial tests of fibre reinforced soil (Prabakar and Sridhar 2002; Patel and Singh 2019). These trends indicate that the optimum fibre length depends on the specimen's size, i.e. fibres will tangle and bend when they are too long for the specimen's size, and their influence cannot be fully mobilised.

Effect of confining pressure on the deviator stress

The influence of confining pressure on the deviator stress of the soil is shown in Table 3. Taking group FRSF as an example, as the confining pressure increases from 50 to 200 kPa, the deviator stress at failure of the specimen (82.8kPa, 133.5 kPa, 205.8 kPa) is 1.77, 1.52 and 1.22 times that of the corresponding URS (46.7kPa, 87.6kPa, 169.1 kPa). The effect of confining pressures on shear strength improvement is analysed by normalising the deviator stress with the effective consolidation pressure for the test (p_0'= 50, 100 and 200 kPa) and the results are shown in Figure 4. It can be seen that the normalised deviator stresses decrease as the confining pressure increases. In Ekinci (2016), when the confining pressure is higher than a threshold value (150 kPa), fibre reinforcement degrades the shear strength of clay. However, no threshold value was found in this study. At higher confining pressures, the soil exhibits stiffer behaviour than at lower confining pressures and the effectiveness of the fibre contribution is reduced, so it is clear that the effect of confining pressure on shear strength improvement is influenced both by the soil's properties and its initial state.

Effect of fibre inclusion on the pore water pressure

As for the excess pore water pressure (PWP), it can be seen from Figure 5 that for all the specimens, the excess PWP experiences a sharp increase at the start of the test, and then increases gradually until it reaches a steady state (0.03 and 0.06 axial strain in Figures 5a and 5b respectively) accompanying further shearing. Finally, a slightly decrease is observed as a result of dilation and minor shear planes in the specimens at higher strain. Similar trends have also been reported by Ekinci (2016) and Khebizi (2019). Also, pore water pressure at both peak and failure increases with increasing fibre inclusion ratio and fibre length. An explanation for this may be that fibres distribute the stresses within the structure of the soil specimen and restrain its dilative deformation tendency, which then leads to an increase in excess pore water pressure.

Effect of fibre inclusion on the strength parameter

The stress paths of URS and selected FRS specimens and fitted critical state lines are shown in Figure 6. Notably, the samples do not fully meet the definition of critical state at the 20% axial strain. However, for the purposes of this study the "critical state line" and "critical state parameter" in the following discussion are used. Generally, the stress paths for URS and FRS show a similar pattern: p' decreases and q increases at the first stage of shearing, so the stress paths plot to the top-left at first. At the second stage, the pore water pressure begins to drop and the deviator stress continues to increase (FRS) or stays constant (URS), so the stress paths then plot to the top-right (FRS) or right (URS). The critical state line is clear for the URS stress paths.

However, FRS stress paths show the influence of confining pressure on the reinforcing effect, reflecting the fact that the stress path at 50 kPa tends to lie above the fitted critical state line and the stress path at 200 kPa tends to lie below the line. An increased *M* value from 1 to 1.36 appears to confirm the shear strength improvement of this soil due to the fibre reinforcement.

4. Derivation and application of a predictive model

As indicated above, and as the title of the paper suggests, the object of this study goes beyond observations made from experimental results and moves towards the development of a simple predictive model with which properties of a fibre-reinforced clay can be predicted. Also as the title suggests, the model proposed here is an initial attempt and for routine use, further work is necessary as will be discussed later.

4.1. Basis of the model

Yang (1972) hypothesised that the improvement of a fibre reinforced soil's shear strength (Δs) comes from "equivalent confining stress" ($\Delta\sigma_3$) induced by tensile restraint in the fibres, i.e. the tensile stresses induced in fibres tend to "add confinement" to the specimen. Gray and Al-Refeai (1986) linked these two terms with a function (Equation 3) based on the friction angle of sandy soil (φ). However, the authors did not give a clear, experimentally available, relationship between $\Delta\sigma_3$ and the properties of the fibre reinforcement.

（3） $\Delta s = \frac{\Delta\sigma_3}{2} \times tan\left(45° + \frac{\varphi}{2}\right).$

The model proposed in this study is based on this concept of "equivalent confining stress" and is based on the following key assumptions:

- The fibre reinforced soil is composed of a soil matrix phase and a fibre phase. The soil matrix phase in fibre reinforced soil is assumed to have the same characteristics as the corresponding unreinforced soil. Both the unreinforced soil and reinforced soil are assumed to follow the critical state framework.
- The soil matrix and fibre-soil composite in the model are homogeneous and isotropic. Fibres are homogeneously distributed in the composite but have a non-uniform orientation distribution. The model is based on shear strengths observed in the CU triaxial tests therefore every point has an identical stress state.
- Fibres are one-dimensional mechanical elements, having the geometry of a cylinder with an average diameter (d_f) and an average length (l_f). Fibres only participate in tension loading and not in compression loading (here the effect of fibre on the consolidation behaviour of the soil is neglected) and behave elastically, with an elastic modulus E_f. Compatibility between fibres and the soil matrix is assumed, i.e. fibres share an identical strain with the adjacent soil matrix as well as the composite due to assumed strong bonding between the clay particles and fibres. Having said this, sliding between fibres and the soil matrix is considered at the end of the model development.
- The radial component of the tensile stress mobilised by fibres is approximately assumed to be the same as and equivalent confining pressure, p_f. ~~the isotropic stress p~~.

The final point above is explained as follows. Due to sample preparation, the preferred orientation of fibres in a triaxial sample will be horizontal and in a triaxial compression test radial expansion would then be resisted by those fibres acting in tension. Considering this effect alone, outside of an actual triaxial test, and assuming elastic behaviour, were the sample to be unrestrained vertically, fibres in tension radially would induce a radial compressive stress and hence vertical tensile strain in the sample via Poisson's ratio. If the sample is restrained such that vertical strain is zero then a vertical stress is induced. If incompressible behaviour is assumed, i.e. Poisson's ratio ν=0.5 then it is easy to show that, elastically, the sample is in a state of hydrostatic stress under these conditions. We can then consider this effect as an "equivalent confining pressure", p_f due to activation of the fibres.

The fibre inclusion ratio has already been defined in Equation 1 and in order to facilitate overall mechanical analysis of the composite, volumetric fibre content is utilised in the model derivation, as shown in Equation 5:

$$(5)\quad v_f = \frac{V_f}{V_t}$$

where V_f and V_t are the volumes of the fibres and composite respectively. The dry unit weight of the fibre-soil composite can be expressed as:

$$(6)\quad \gamma_{dFRS} = \frac{W_f + W_s}{V_t}$$

the specific gravity of the fibres can be expressed as:

$$(7)\quad G_f = \frac{W_f}{V_f \gamma_w}$$

where γ_w is the unit weight of water. The relationship between gravimetric fibre content ρ_f and volumetric fibre content v_f can be obtained by substituting Equations 5 to 6 into Equation 7, i.e.

$$(8)\quad v_f = \frac{\gamma_{dFRS}\rho_f}{(1+\rho_f)G_f\gamma_w}.$$

4.2. Model derivation

For a single fibre inclined to the horizontal plane at an angle θ, the strain of a single fibre in the direction of the fibre axis (assuming a straight portion of fibre), $\varepsilon^{l}{}_{f}(\theta)$, can be decomposed into strains in the radial (ε_r) and axial directions (ε_a) as follows:

$$\varepsilon_f^1(\theta) = \varepsilon_a \sin^2\theta + \varepsilon_r \cos^2\theta. \tag{9}$$

In a CU test, the volumetric strain, ε_v is zero so that

$$\varepsilon_v = \varepsilon_a + 2\varepsilon_r = 0 \tag{10}$$

$$\varepsilon_r = -\frac{1}{2}\varepsilon_a. \tag{11}$$

Substituting Equation 11 into Equation 9 gives

$$\varepsilon_f^1(\theta) = \varepsilon_a(\sin^2\theta - \frac{1}{2}\cos^2\theta). \tag{12}$$

The stress in a single fibre in the fibre direction $\sigma^1_f(\theta)$ is

$$\sigma_f^1(\theta) = E_f \varepsilon_f^1(\theta) \tag{13}$$

where E_f is the elastic modulus of the fibre material. The contribution of a single fibre to the stress in the radial direction, $\sigma^1_{rf}(\theta)$, can be derived via a similar approach in Diambra (2010) by decomposing, $\sigma^1_f(\theta)$ into terms associated with work done which can be expressed as

$$\sigma_{af}^1(\theta)\varepsilon_a + 2\sigma_{rf}^1(\theta)\varepsilon_r = \sigma_f^1(\theta)\varepsilon_f^1(\theta) \tag{14}$$

$$\sigma_f^1(\theta)\varepsilon_f^1(\theta) = \sigma_f^1(\theta)(\sin^2\theta\,\varepsilon_a + \cos^2\theta\,\varepsilon_r) \tag{15}$$

where $\sigma^1_{af}(\theta)$ and $\sigma^1_{rf}(\theta)$ are the stresses in a single fibre in axial and radial directions respectively. So the stress decomposition in the radial direction is

$$\sigma_{rf}^1(\theta) = \sigma_f^1(\theta)\frac{1}{2}\cos^2\theta = E_f \times \varepsilon_a(\frac{1}{2}\sin^2\theta\cos^2\theta - \frac{1}{4}\cos^4\theta). \tag{16}$$

As mentioned above, only the stress in the radial direction is considered. Then the tensile force carried by a single fibre in the radial direction, $F^1_{rf}(\theta)$, can be calculated by multiplying the stress in the radial direction by the projected area of the fibre, i.e.

$$F_{rf}^1(\theta) = \sigma_{rf}^1(\theta)\frac{A_f^1}{\cos\theta} \tag{17}$$

where A^1_f is the cross-sectional area of a single fibre.

Calculating the total tensile force carried by all fibres requires integration of all fibre forces. An approach similar to that proposed by Michalowski and Cermak (2003) is used here. The fibres are randomly distributed in the specimen (Figure 7a), and the stress and strain conditions at every point in the triaxial specimen are assumed identical. The fibres are assumed to have a uniform distribution in the horizontal plane (α). Hence the strains in the fibres depend only on their inclination angle to the horizontal (θ), and are independent of fibres' positions. So all fibres can be moved together, making the midpoints of fibres coincide (Figure 7b), and spherical coordinates (Figure 7c) are used as the integration space in order to calculate the contribution of all fibres in the specimen. The volume of the sphere containing the fibres, V is

$$V = \frac{4}{3}\pi\left(\frac{1}{2}l_f\right)^3 \tag{18}$$

and the infinitesimal volume required to undertake the integration can be expressed by the fibre length l_f and the orientation of the fibre (α and θ)

$$\mathrm{d}V = \frac{1}{3}\left(\frac{1}{2}l_f\right)^3 d\theta d\alpha \cos\theta. \tag{19}$$

Since it is almost impossible to determine the actual arrangement condition of fibres in a given specimen, by considering the preferred sub-horizontal orientation of fibres, the distribution function proposed by Michalowski (1997) is applied here, i.e.

$$\rho(\theta) = \frac{3}{2}\cos^2\theta\rho_{ave} \tag{20}$$

where $\rho(\theta)$ represents the volumetric fibre content with an orientation angle θ above the horizontal plane in an infinitesimal volume dV (Figure 7c). ρ_{ave} is the average volumetric fibre content in the sphere, where

$$\rho_{ave} = \frac{V_f}{V}. \tag{21}$$

It is worth noting that for a given fibre reinforced soil specimen, ρ_{ave} is not the same as v_f in value because the volume of the specimen (V_t) is not the same as the volume of the integration space (V). ρ_{ave} also depends on V_t. For a fibre reinforced specimen with a volume V_t, the relationship below can be obtained from Equations 20 and 21,

$$\frac{3}{2} cos^2 \theta \, \rho_{ave} = \frac{3}{2} cos^2 \theta \frac{V_f}{V_t} \times \frac{V_t}{V} = \frac{V_f^\theta}{dV} \times \frac{V_t}{V} \tag{22}$$

$$\rho(\theta) = \frac{V_f^\theta}{dV} \times \frac{V_t}{V} \tag{23}$$

where $V^\theta{}_f$ is the total fibre volume with an orientation angle θ above the horizontal plane in a fibre reinforced soil specimen. For all the fibres with an orientation angle θ above the horizontal plane, the total tensile force in radial direction $F_{rf}(\theta)$ can be calculated using equilibrium as

$$F_{rf}(\theta) = \sigma_{rf}^1(\theta) \frac{A_f^1}{cos\,\theta} N(\theta) \tag{24}$$

where $N(\theta)$ is the number of fibres at angle θ above the horizontal plane, which can be expressed as

$$F_{rf}(\theta) = \sigma_{rf}^1(\theta) \frac{A_f^\theta}{cos\,\theta} = \sigma_{rf}^1(\theta) \frac{V_f^\theta}{l_f \, cos\,\theta} \tag{25}$$

where $A^\theta{}_f$ is total cross sectional area of fibres at angle θ.

Substituting Equations 20 and 23 into Equation 25, one can obtain the following

$$F_{rf}(\theta) = \sigma_{rf}^1(\theta) \frac{\frac{3}{2} cos\,\theta \, \rho_{ave} dV}{l_f}. \tag{26}$$

Assuming the horizontal distribution (α in Figure 7c) of fibres in the specimen is homogenous, and the vertical distribution (θ in Figure 7c) of fibres in the specimen is followed, i.e. $\rho(\theta)$ in Equation 20, the total fibre tensile force in the radial direction in specimen is:

$$F_{rf} = \int_V \sigma_{rf}^1(\theta) \frac{\frac{3}{2} cos\,\theta \, \rho_{ave}}{l_f} dV \tag{27}$$

and Equation 27 can be expanded to

(28) $$F_{rf}=\frac{1}{l_f}\frac{\pi}{8}E_f {l_f}^3\rho_{ave}\varepsilon_a\int_{-\frac{\pi}{2}}^{\frac{\pi}{2}}\left(\frac{1}{2}sin^2\theta\, cos^4\theta-\frac{1}{4}cos^6\theta\right)d\theta.$$

As mentioned previously, in a triaxial compression test, only those fibres acting in tension contribute to generated confining stress. Hence the integration in Equation 28 should be performed with upper and lower limits. Similar to Diambra (2010), the limit angle θ_0 (Figure 6a) can be determined by decomposing the strain. According to a Mohr's circle for a strain increment, only the tensile zone ($d\varepsilon_\theta<0$) should be considered. So by letting Equation 9 be zero, θ_0 can be obtained as

(29) $$\theta_0=tan^{-1}\sqrt{-\frac{d\varepsilon_r}{d\varepsilon_a}}.$$

Substituting Equation 11 into Equation 29, it can be shown that $\theta_0=tan^{-1}\sqrt{\frac{1}{2}}$.

So the integration part of Equation 28 can now be rewritten as

(30) $$\int_{-tan^{-1}\sqrt{\frac{1}{2}}}^{tan^{-1}\sqrt{\frac{1}{2}}}\left(\frac{1}{2}sin^2\theta\, cos^4\theta-\frac{1}{4}cos^6\theta\right)d\theta.$$

Equation 30 can be obtained by numerical quadrature of the function curve, the result is approximately 0.174 in value. In a triaxial test, the equivalent confining pressure can be estimated by applying the total tensile force on the lateral surface (S_l) of the specimen, which can be expressed as

(31) $$S_l=2\pi RH$$

where R and H are radius and height of the specimen respectively.

So the equivalent confining pressure induced by the fibres is

(32) $$p_f=\frac{F_{rf}}{S_l}=\frac{0.174\frac{\pi}{8}E_f {l_f}^3\rho_{ave}\varepsilon_a}{2\pi RHl_f}=\frac{0.065Rv_fE_f}{l_f}\varepsilon_a.$$

It is worth mentioning that here isotropic stress p_f is assumed equal to the radial component of the fibre stress action on the specimen according to the last point of the assumptions (as clarified previously).

Let $\frac{0.065Rv_fE_f}{l_f}$ be the parameter, P_f (kPa), Equation 32 can then be expressed as

$$(33)\quad p_f = P_f\varepsilon_a.$$

It can be seen from Equation 33 that for a given fibre reinforced soil specimen, the model developed above predicts equivalent confining pressure to increase linearly with the increasing axial compressive strain of the sample. Table 4 gives the relationship between P_f and fibre inclusion ratio v_f and fibre length l_f, as well as other parameters in the model. The soil names in Table 4 are consistent with Table 3.

Table 4. Input parameters and P_f for different fibre reinforced specimens.

Soil type	FRSA	FRSB	FRSC	FRSD	FRSE	FRSF
v_f (%)	0.5	1.0	1.49	0.5	1.0	1.49
l_f (mm)	6	6	6	12	12	12
E_f (MPa)	2000	2000	2000	2000	2000	2000
R (mm)	19	19	19	19	19	19
H (mm)	76	76	76	76	76	76
P_f (kPa)	2058.3	4116.6	6133.8	1029.1	2058.3	3066.9

A modified parameter, α_f, is introduced in the form of Equations 34 and 35 to describe the sliding effect and to take account of the various behaviours seen in the triaxial tests of fibre reinforced soils presented previously. Four material parameters are introduced as justified below and later, the triaxial results are used to provide calibration. After this, the model is used to predict strength behaviour, again with comparison to the triaxial test results from this study and other investigations.

$$(34)\quad \alpha_f = \left[(\varepsilon_a)^{\alpha}\left(\frac{\beta}{-\ln B_f}\right)\left(\frac{p_{ref}}{p_0'}\right)^{\gamma}\left(\frac{\rho_f}{\rho_f^{ref}}\right)^{\chi}\right]$$

$$(35)\quad B_f = \frac{l_f}{l_f^{ref}}$$

where sliding parameter (α), confining pressure parameter (γ), fibre inclusion ratio parameter (χ) and geometry parameter (β) are introduced to modify the model. The effective consolidation pressure (p_0'), fibre content (ρ_f) and fibre length (l_f) are normalised by the reference values p_{ref} (50 kPa), ρ_f^{ref} (0.1%) and l_f^{ref} (20mm) respectively, the p_{ref} and ρ_f^{ref} were selected as they are the minimum value can be found in most of the experimental study according to the literature review. l_f^{ref} is close to the half of the diameter of the specimen (38mm), which is the maximum value of fibre length in most of the studies.

4.3. Model calibration and application

The four introduced parameters in the model are calibrated with the triaxial test results in this study, the results are shown in Figures 8-11, and the process of calibration is introduced as follows. Sliding factor α accounts for the sliding effect; the decrease of the rate of shear strength improvement (Δq in Figure 3) means the equivalent confining pressure is reduced with respect to the axial strain due to the relative sliding. α is calibrated here separately by considering the Δq, as shown in Equation 36 (the details will be introduced later):

$$\Delta q = 3p_f = 3(\varepsilon_a)^{\alpha} P_f \varepsilon_a \quad (36)$$

It can be seen from Figure 8 that when α is closer to 0, the sliding effect is more obviously and the relationship between strength improvement and axial strain is more linear. By considering the test results shown in Figures 3, α is set as -0.63 in the model.

β accounts for the fibre length effect and the test results indicate that longer fibres have better behaviour in improving the shear strength of the soil. The influence of β on the predicted results is shown in Figure 9. It can be seen that the difference between 12 mm and 6 mm fibres gets greater as β increases. β is therefore set as 0.006 by considering the effect of fibre length in this study. The effect of the variation of fibre inclusion ratio parameter (χ) on the predicted results can be seen in Figure 10. The observed triaxial test results show that as the fibre inclusion ratio increases, the benefit of fibre reinforcement is not proportional to the increment of fibre inclusion ratio. When γ decreases from 0, a decreased reinforcing benefit at higher fibre inclusion ratio is more obvious. According to the observed trend the fibre inclusion ratio parameter χ is set as -0.05.

Figure 11 shows the calibration of confining pressure parameter (γ). The increased confining pressure does not lead to a proportional increment in deviator stress (the reinforcing benefit is decreased), as γ increases from 0, this trend becomes stronger. According to the observed trend the confining pressure parameter γ is set as 0.15. The calibrated parameters can be used to calculated the modified equivalent confining pressure (p_f^*) via Equation 37, and the application of the model is introduced in the following section.

$$(37)\quad p_f^* = \alpha_f P_f \varepsilon_a.$$

4.4 Applying the model

The process of using this model to predict the shear strength behaviour of fibre reinforced clay is now discussed. As mentioned above, the effect of fibre reinforcement is modelled as an equivalent confining pressure acting on the specimen in the triaxial test. For the total stress path results of unreinforced and reinforced specimens, the mean stress difference is considered to be p_f for which there is a corresponding difference in final deviator stress (q_f). For the fibre reinforced soil, the mean stress (p_{frs}) and deviator stress (q_{frs}) of any point in the test can be considered as the combination of mean stresses in the unreinforced case and an effective confining pressure from the presence of fibres, i.e.

$$p_{frs} = p_{urs} + p_f \tag{38}$$

$$q_{frs} = q_{urs} + q_f = q_{urs} + 3p_f \, . \tag{39}$$

Clearly for a given sample p_{urs} and q_{urs} can be obtained from a triaxial test, so once the equivalent confining pressure is calculated, the model can deliver the total stress path and stress-strain relationships for the same sample when reinforced with fibres. The selected experimental measured (Exp.) results in this study and corresponding model predicted (Mod.) deviator stress-axial strain curves are shown in Figures 12. It can be seen the model is capable of good predictions of the stress-strain behaviour in this study.

In order to evaluate the model, tests results on fibre reinforced clay from Correia et al. (2021) and Babu and Chouksey (2010) are also introduced. The predicted results of these studies via the model and the experimental results are compared in Figures 13. It can be seen from Figure 13a that the model predicted results make good agreement with the experimental results when the confining pressure is 50 and 100 kPa. When the confining pressure is 300 kPa, the model tends to underestimate the fibre reinforced soil when the axial strain is greater than 12%.

In Figure 13b, the predicted results via model proposed in Babu and Chouksey (2010) are also shown. Comparing with the model in Babu and Chouksey (2010), the proposed model in this study underestimates the deviator stress when the fibre inclusion ratio increases to 1% and 2%. This is due to the inclusion ratio parameter (χ) leads to a decrease in deviator stress improvement when the fibre inclusion ratio is high. However, this trend is not observed in Babu and Chouksey

(2010). Also, the strain scale in these tests (15%) is not the same as that in this study (20%), which means the sliding factor (α) might lead to some inaccuracy, it can be seen that the predicted results get closer to the experimental data as the strain increases, so it can be deduced that this model appears to be in better agreement with the data at large strains.

Comparing with the model proposed in Babu and Chouksey (2010), the model proposed in this study does not need any interface parameters between materials. Once the geometry and mechanical data of the fibre are known and the confining pressure and fibre inclusion ratio are set, one can obtain the stress-strain relationship of the fibre reinforced soil. This model can also be used in predicting the pore water pressure-strain relationship of fibre reinforced soil as shown in the following.

According to Skempton (1954), the pore water pressure change for a saturated specimen during an undrained triaxial test can be expressed as

（40） $$\Delta u = B\left[\Delta\sigma_3 + A(\Delta\sigma_3 - \sigma_1)\right]$$

where B is 1 and $\Delta\sigma_3$ is 0 during the CU test and A is the pore water pressure coefficient, which changes during the test and depends on the stress level. It can be expressed as the current slope of the q-u curve. For fibre reinforced soil, the excess pore water pressure generated during the tests (Δu_{frs}) can be considered as a combination of that which occurs in an unreinforced soil (Δu_{urs}) and a component due to the fibre reinforcement (Δu_f). Assuming the coefficient A of FRS is the same as that of URS and according to Equation 40, Δu_{frs} can be expressed as

（41） $$\Delta u_{frs} = \Delta u_{urs} + \Delta u_f = \Delta u_{urs} + \frac{\Delta u_{urs}}{\Delta q_{urs}}\Delta q_f = \frac{\Delta u_{urs}}{\Delta q_{urs}}\Delta q_{frs} .$$

A series of pore water pressure coefficients A can therefore be calculated based on the test results of unreinforced soil at different confining pressures, therefore the excess pore water pressure-strain relationships for a fibre reinforced soil can be obtained as per Equation 41. The effective stresses can then be obtained following Terzaghi's principle.

The experimental measured and model predicted pore water pressure-strain curves in this study are shown in Figure 14. It can be seen the model is capable of good predictions of the relationships generally. When the confining pressure is 200 kPa, the model tends to overestimate pore water pressures for fibre reinforced soil samples when the axial strain is in the range of 7% to 15%. This is attributed to the pore water pressure coefficient A, which obtained from the URS tests.

In Figure 15, the predicted results and experimental results in Babu and Chouksey (2010) are compared. It can be seen that the predicted results via the model in this study are more similar in pattern with the experimental data, although the model tends to underestimate the excess pore water pressure value of fibre reinforced soil. Hence, it can be concluded that the proposed model makes reasonable predictions of the triaxial test behaviour on fibre reinforced soils at different confining pressures.

5. Conclusion

In this study, the shear strength of polypropylene fibre reinforced London Clay was evaluated via a series of CU triaxial tests. Based on the tests results, a practical predictive model is proposed using the equivalent confining stress concept. A summary of the conclusions drawn from the results and discussions is presented below:

(1) Polypropylene fibre can significantly increase the shear strength behaviour of London Clay. The shear strength of the soil increases with increasing fibre inclusion ratio and fibre length due to the higher pull out resistance. Higher fibre inclusion ratio and fibre length also resultin higher pore water pressure during the shearing.

(2) Fibre addition can increase the hardening behaviour of the stress-strain response of the soil. As the axial strain increases, for the unreinforced soil, the deviator stress tends to increase and then keep steady until the axial strain reaches 20%. For the fibre reinforced soil, the deviator increases throughout the test and does not show a peak value before the test is finished.

(3) A speculative model is proposed based on the equivalent confining stress conception to predict the shear strength behaviour of fibre reinforced clay, where the model considers the effect of fibre reinforcement as an equivalent confining pressure which then leads to greater shear strength, the behaviour of fibre reinforced soils can be predicted by the superposition of unreinforced soil and fibre contributions. The model has a satisfactory performance in predicting the stress-strain, pore water pressure-strain relationships of the fibre reinforced soil.

(4) This model can be used as a tool to predict the shear strength of fibre reinforced clay in geotechnical engineering practice without requiring specialist and costly laboratory testing programmes. More experiments of different clay reinforced with different fibre inclusion ratios, fibre lengths and confining pressures can be utilized to make the model more comprehensive.

Acknowledgements

Contributors' statement

Jianye Wang: Conceptualization, Investigation, Methodology, Data Curation, Visualization, Writing-Original Draft; **Paul N Hughes**: Resources, Methodology, Writing-review & editing, Supervision, Validation; **Charles E Augarde**: Methodology, Writing-review & editing, Supervision, Formal analysis

Funding statement

This research was supported by China Scholarship Council (grant No. 201608110138) and the UK Engineering and Physical Sciences Research Council (EPSRC) via the ACHILLES project (grant No. EP/R034575/1).

Declaration of interest statement

The authors declare there are no competing interests.

Data availability statement

The data to support this study will be made available at a DOI once the manuscript has been accepted.

References

ADFIL (2019) Product data. See: http://www.adfil.com/products/microsynthetic-fibres/monofilament-fibres, (accessed 25/06/2019).

Ajayi, O., Le Pen, L., Zervos, A. and Powrie, W. 2016. A behavioural framework for fibre reinforced gravel. Géotechnique, **67**(1): 56-68. doi:10.1680/jgeot.16.P.023.

Akbulut, S., Arasan, S. and Kalkan, E. 2007. Modification of clayey soils using scrap tire rubber and synthetic fibers. Applied Clay Science, **38**(1-2): 23-32. doi:10.1016/j.clay.200 7.02.001.

Aouali, N., Benessalah, I., Arab, A., Ali, B. and Abed, M. 2019. Shear strength response of fibre reinforced Chlef (Algeria) silty sand: laboratory study. Geotechnical and Geological Engineering, **37**(2): 1047-1057. doi:10.1007/s10706-018-0641-5.

Babu, G. S., & Chouksey, S. K. 2010. Model for analysis of fiber-reinforced clayey soil. Geomechanics and Geoengineering, **5**(4): 277-285. doi:10.1080/17486021003706804

Briggs, K., 2010. Charing embankment: climate change impacts on embankment hydrology. Ground Engineering, **43**(6):28-31.

Briggs, K.M., Loveridge, F.A. and Glendinning, S. 2017. Failures in transport infrastructure embankments. Engineering Geology, **219**: 107-117. doi:10.1016/j.enggeo.2016.07.016.

BSI. 1990. BS-1377-2: Methods of test for soils for civil engineering purposes- Classification tests. BSI, London, UK.

BSI. 1990. BS 1377-4: Methods of test for soils for civil engineering purposes Compaction related tests. BSI, London, UK.

BSI. 1990. BS 1377-8: Methods of test for soils for civil engineering purposes Shear strength tests (effective stress). BSI, London, UK.

Consoli, N.C., da Silva, A.P., Nierwinski, H.P. and Sosnoski, J. 2018. Durability, strength, and stiffness of compacted gold tailings-cement mixes. Canadian Geotechnical Journal, **55**(4): 486-494. doi:10.1139/cgj-2016-0391.

Correia, N.S., Rocha, S.A., Lodi, P.C. and McCartney, J.S., 2021. Shear strength behavior of clayey soil reinforced with polypropylene fibers under drained and undrained conditions. Geotextiles and Geomembranes, **48**: (In press). doi:10.1016/j.geotexmem.2021.05.005.

Chen, C.W. 2007. A constituitive model for fiber-reinforced soils. Ph.D. dissertation, University of Missouri-Columbia.

Diambra, A. 2010. Fibre reinforced sands: experiments and constitutive modelling. Ph.D. dissertation, University of Bristol.

Diambra, A., Ibraim, E., Wood, D.M. and Russell, A.R. 2010. Fibre reinforced sands: experiments and modelling. Geotextiles and geomembranes, **28**(3): 238-250. doi:10.1016/j.geotexmem.2009.09.010.

Diambra, A. and Ibraim, E. 2014. Modelling of fibre–cohesive soil mixtures. Acta Geotechnica, **9**(6): 1029-1043. doi:10.1007/s11440-013-0283-y.

Ekinci, A., 2016. The mechanical properties of compacted clay from the Lambeth Group using fibre reinforcement. Ph.D. dissertation, University College London.

El Mountassir, G., Sánchez, M., Romero, E. and Soemitro, R.A., 2011. Behaviour of compacted silt used to construct flood embankment. Proceedings of the Institution of Civil Engineers-Geotechnical Engineering, 164(3): 195-210. doi:10.1680/geng.10.00055.

Foresta, V., Capobianco, V. and Cascini, L. 2020. Influence of grass roots on shear strength of pyroclastic soils. Canadian Geotechnical Journal, **57**(9): 1320-1334. doi:10.1139/cgj-2019 -0142.

Gao, Z. and Diambra, A. 2020. A Multiaxial Constitutive Model for Fibre-reinforced Sand. Géotechnique, **71**(6): 548-560. doi:10.1680/jgeot.19.P.250.

Gao, Z. and Zhao, J. 2012. Evaluation on failure of fiber-reinforced sand. Journal of Geotechnical and Geoenvironmental Engineering, **139**(1): 95-106. doi:10.1061/(ASCE)GT.1943-5606.0000737.

Gray, D.H. and Al-Refeai, T. 1986. Behavior of fabric-versus fiber-reinforced sand. Journal of Geotechnical Engineering, **112**(8): 804-820. doi: 10.1061/(ASCE)0733-9410(1986)112:8(804).

Gray, DH and Ohashi, H. 1983. Mechanics of fiber reinforcement in sand. Journal of Geotechnical Engineering, **109**(3): 335-353. doi:10.1061/(ASCE)0733-9410(1983)109:3 (335).

Gunn, D.A., Chambers, J.E., Uhlemann, S., Wilkinson, P.B., Meldrum, P.I., Dijkstra, T.A., Haslam, E., Kirkham, M., Wragg, J., Holyoake, S. and Hughes, P.N. 2015. Moisture monitoring in clay embankments using electrical resistivity tomography. Construction and Building Materials, **92**: 82-94. doi:10.1016/j.conbuildmat.2014.06.007.

Han, C., He, Y., Tian, J., Zhang, J., Li, J. and Wang, S. 2020. Shear strength of polypropylene fibre reinforced clay. Road Materials and Pavement Design, **21**: 1-18. doi:10.1080/14680629.2020.1798807.

Hazirbaba, K. 2018. Large-scale direct shear and CBR performance of geofibre-reinforced sand. Road Materials and Pavement Design, **19**(6): 1350-1371. doi:10.1080/14680629.2017.1310667.

IPCC. 2014. Climate Change 2014: Synthesis Report. Contribution of Working Groups I, II and III to the Fifth Assessment Report of the Intergovernmental Panel on Climate Change. Pachauri, R.K. and Meyer, L.A. IPCC, Geneva, Switzerland.

Jamei, M., Villard, P. and Guiras, H. 2013. Shear failure criterion based on experimental and modeling results for fiber-reinforced clay. International Journal of Geomechanics, **13**(6): 882-893. doi:10.1061/(ASCE)GM.1943-5622.0000258.

Kalkan, E. 2013. Preparation of scrap tire rubber fiber-silica fume mixtures for modification of clayey soils. Applied Clay Science, **80**: 117-125. doi:10.1016/j.clay.2013.06.014.

Karimzadeh, A.A., Leung, A.K., Hosseinpour, S., Wu, Z. and Fardad Amini, P. 2021. Monotonic and cyclic behaviour of root-reinforced sand. Canadian Geotechnical Journal, **58**: (In press).doi:10.1139/cgj-2020-0626.

Khan, M.S., Hossain, S., Ahmed, A. and Faysal, M. 2017. Investigation of a shallow slope failure on expansive clay in Texas. Engineering Geology, **219**: 118-129. doi:10.1016/j.enggeo.2016. 10.004.

Khebizi, W., Della, N., Denine, S., Canou, J. and Dupla, J.C. 2019. Undrained behaviour of polypropylene fibre reinforced sandy soil under monotonic loading. Geomechanics and Geoengineering, **14**(1): 30-40. doi:10.1080/17486025.2018.1508855.

Mandolini, A., Diambra, A. and Ibraim, E. 2019. Strength anisotropy of fibre-reinforced sands under multiaxial loading. Géotechnique, **69**(3): 203-216. doi:10.1680/jgeot.17.P.102.

Mirzababaei, M., Arulrajah, A., Horpibulsuk, S. and Aldava, M. 2017. Shear strength of a fibre-reinforced clay at large shear displacement when subjected to different stress histories. Geotextiles and Geomembranes, **45**(5): 422-429. doi:10.1016/j.geotexmem.2017.06.002.

Mirzababaei, M., Arulrajah, A., Haque, A., Nimbalkar, S. and Mohajerani, A. 2018. Effect of fiber reinforcement on shear strength and void ratio of soft clay. Geosynthetics International, **25**(4): 471-480. doi:10.1680/jgein.18.00023.

Michalowski, R.L. 1997. Limit stress for granular composites reinforced with continuous filaments. Journal of Engineering Mechanics, **123**(8): 852-859. doi:10.1061/(ASCE)0733 - 9399(1997)123:8(852).

Michalowski RL and Cermak J. 2003. Triaxial compression of sand reinforced with fibers. Journal of Geotechnical and Geoenvironment Engineering, **129**(2): 125-136. doi:10.1061/(ASCE) 1090-0241(2003)129:2(125).

Michalowski, R.L. and Zhao, A. 1996. Failure of fiber-reinforced granular soils. Journal of Geotechnical Engineering, **122**(3): 226-234. doi:10.1061/(ASCE)0733-9410(1996)122:3(226).

Ni, J., Li, S.S., Ma, L. and Geng, X.Y. 2020. Performance of soils enhanced with eco-friendly biopolymers in unconfined compression strength tests and fatigue loading tests. Construction and Building Materials, **263**: p.120039. doi:10.1016/j.conbuildmat.2020.120039.

Ni, J., Li, S.S. and Geng, X.Y. 2022. Mechanical and biodeterioration behaviours of a clayey soil strengthened with combined carrageenan and casein. Acta Geotechnica, **17**: 5411–5427. doi:10.1007/s11440-022-01588-4.

Patel, S.K. and Singh, B. 2019. Shear strength response of glass fibre-reinforced sand with varying compacted relative density. International Journal of Geotechnical Engineering, **13**(4): 339-351. doi:10.1080/19386362.2017.1352157.

Prabakar, J. and Sridhar, R.S. 2002. Effect of random inclusion of sisal fibre on strength behaviour of soil. Construction and Building materials, **16**(2): 123-131. doi:10.1016/S0950-0618(02) 00008-9.

Taha, M.M., Feng, C.P. and Ahmed, S.H. 2020. Influence of polypropylene fibre (PF) reinforcement on mechanical properties of clay soil. Advances in Polymer Technology, **2020**:1-15. doi:10.1155/2020/9512839.

Tang, A.M., Hughes, P.N., Dijkstra, T.A., Askarinejad, A., Brenčič, M., Cui, Y.J., Diez, J.J., Firgi, T., Gajewska, B., Gentile, F. and Grossi, G. 2018. Atmosphere vegetation soil interactions in a climate change context; impact of changing conditions on engineered transport infrastructure slopes in Europe. Quarterly journal of engineering geology and hydrogeology. **51**(2): 156-168. doi:10.1144/qjegh2017-103.

Wang, J.Y. 2020. The engineering properties and mechanical behaviour of fibre reinforced clay. Ph.D. dissertation, Durham University.

Wang, Y., Guo, P., Dai, F., Li, X., Zhao, Y. and Liu, Y. 2018. Behavior and modeling of fiber-reinforced clay under triaxial compression by combining the superposition method with the energy-based homogenization technique. International Journal of Geomechanics, **18**(12): 04018172. doi:10.1061/(ASCE)GM.1943-5622.0001313.

Yang, Z. 1972. Strength and deformation characteristics of reinforced sand. Ph.D. dissertation, University of California.

Yu, J., Chen, Y., Chen, G. and Wang, L. 2020. Experimental study of the feasibility of using anhydrous sodium metasilicate as a geopolymer activator for soil stabilization. Engineering Geology, **264**: 105316. doi:10.1016/j.enggeo.2019.105316.

Zornberg, J.G. 2002. Discrete framework for limit equilibrium analysis of fibre-reinforced soil. Géotechnique, **52**(8): 593-604. doi:10.1680/geot.2002.52.8.593.

List of symbols

Symbol	Definition
A_f^1	cross section area of single fibre
A_f^θ	total cross section area of fibres in θ
D_{50}	median diameter of soil

d_f	diameter of fibre
e_0	Initial void ratio
E_f	elastic modulus of fibre
$F_{rf}^1(\theta)$	tensile force in radial direction carried by single fibre
$F_{rf}(\theta)$	total tensile force in radial direction carried by fibres in θ
F_{rf}	total tensile force in radial direction carried by all fibres
H	height of triaxial specimen
l_f	fibre length
$l_f^{\ ref}$	reference fibre length
m_s	mass of the fibre
m_f	mass of the dry soil
$N(\theta)$	number of fibres in θ
p	mean stress
p_{ref}	reference pressure
p_f	equivalent confining pressure induced by all fibres
p_f^*	calibrated equivalent confining pressure
p'	mean effective stress
p'_0	effective consolidation pressure
q	deviator stress
R	radius of specimen
S_l	lateral surface of specimen
u	pore water pressure
V	total volume of fibre sphere
V_f	volume of fibres

V_t total volume of specimen

V_f^{θ} total fibre volume in direction θ

$\alpha, \beta, \chi, \gamma$ parameters of the model

ε_a axial strain

ε_r radial strain

$\varepsilon_f^1(\theta)$ single fibre strain in fibre direction

θ_0 limit incline angle of effective fibres in specimen

v_f volumetric fibre inclusion ratio

ρ_f^{ref} reference gravimetric fibre inclusion ratio

ρ_f gravimetric fibre inclusion ratio

$\rho(\theta)$ volumetric fibre concentration in direction θ

ρ_{ave} average volumetric fibre concentration in sphere

σ_1 major principal stress

σ_3 minor principal stress

$\sigma_f^1(\theta)$ single fibre stress in fibre direction

$\sigma_{af}^1(\theta)$ single fibre strain in axial direction

$\sigma_{rf}^1(\theta)$ single fibre strain in radial direction

Figures:

Figure 1

Figure 2 (a) and (b)

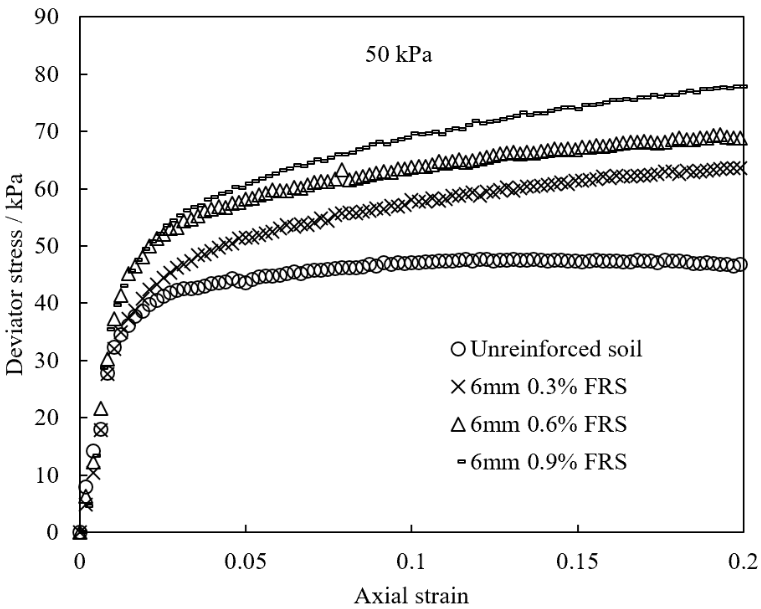

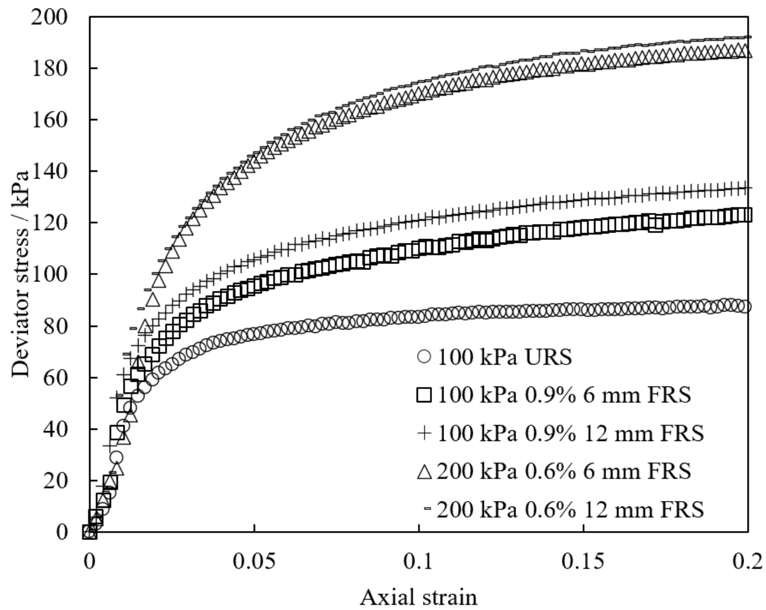

Figure 3

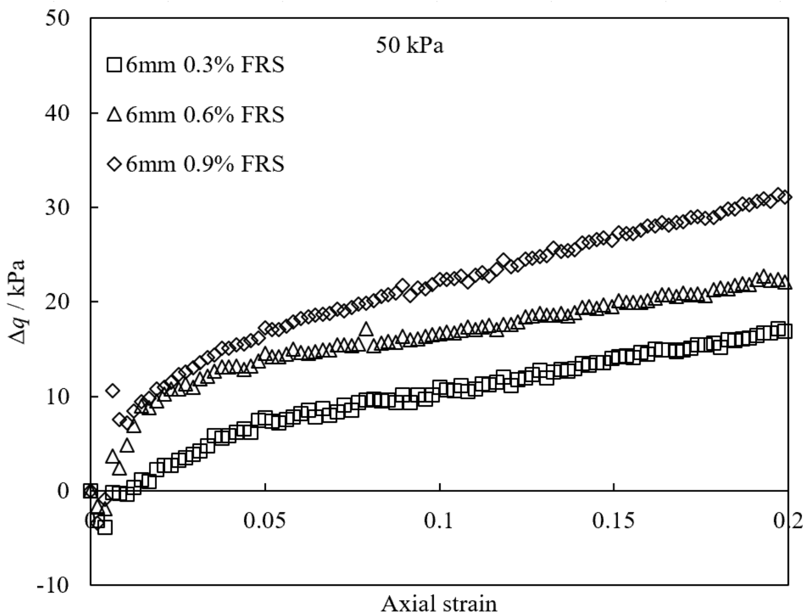

Figure 4

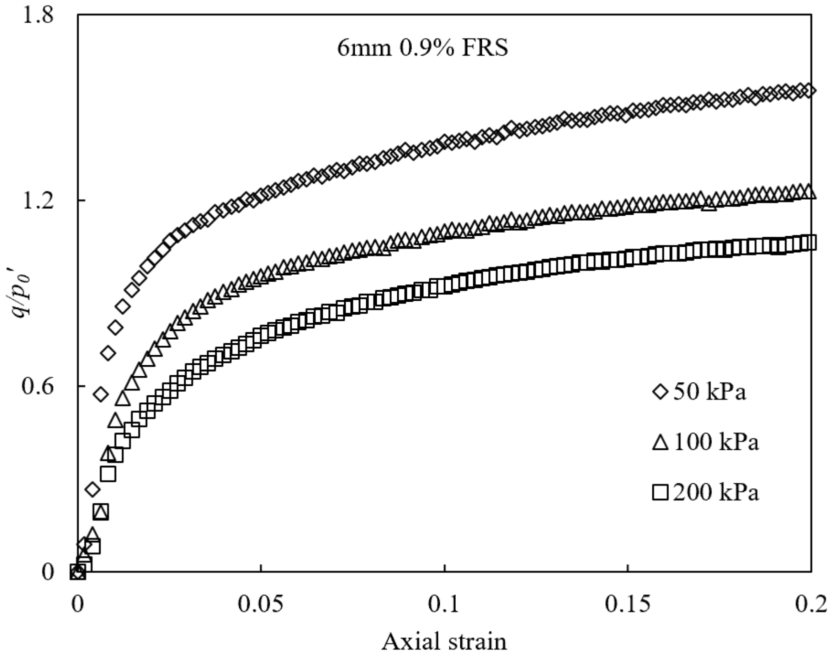

Figure 5 (a) and (b)

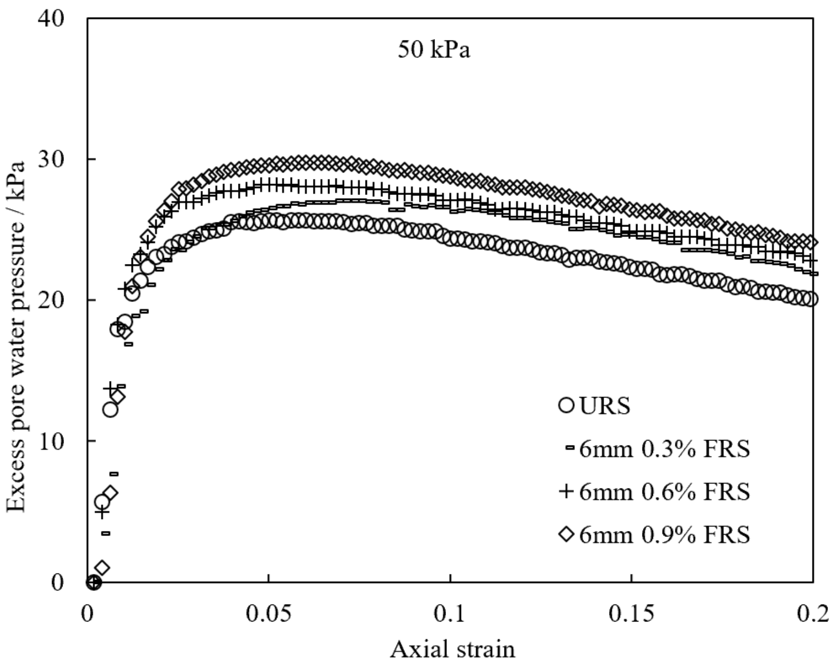

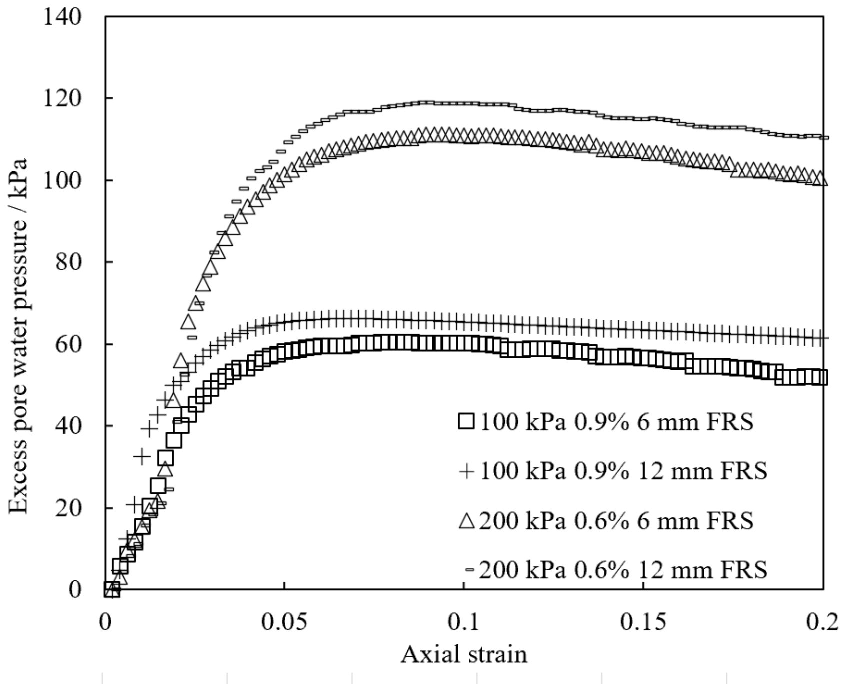

Figure 6

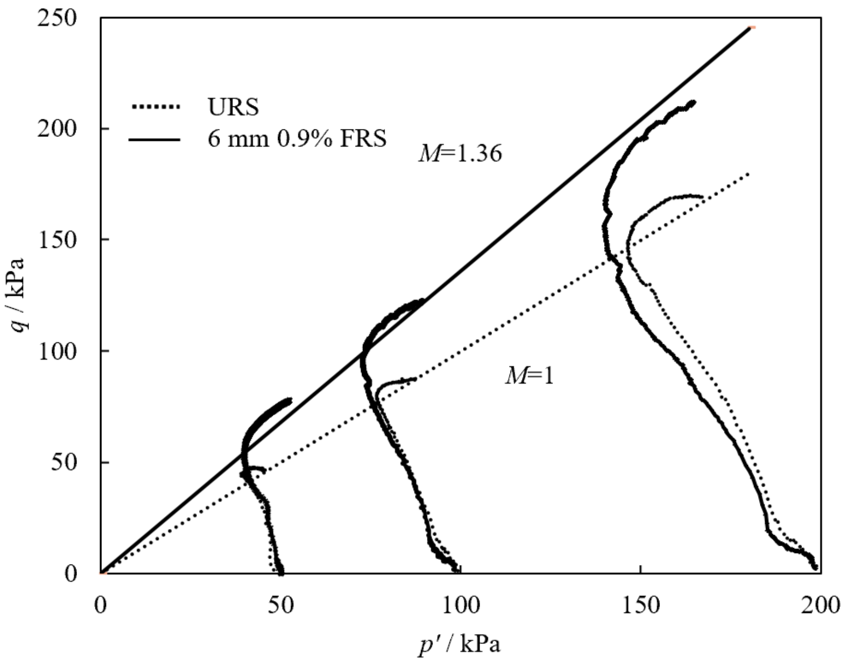

Figure 7 (a), (b) and (c)

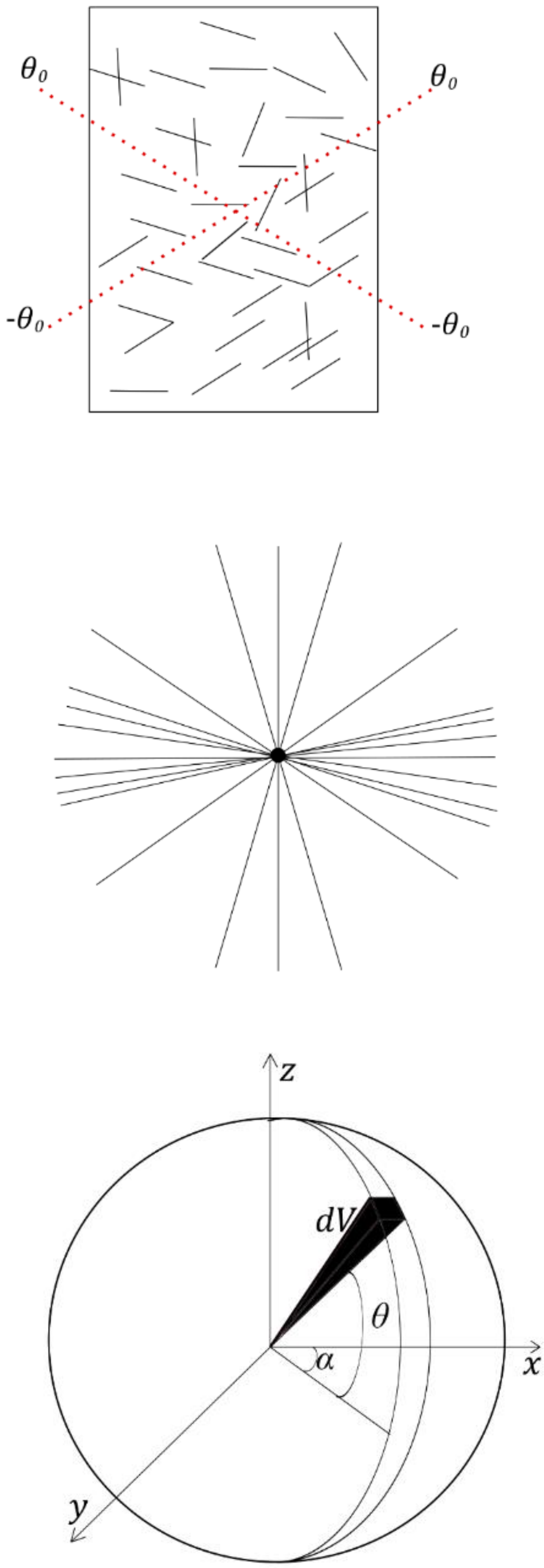

Figure 8

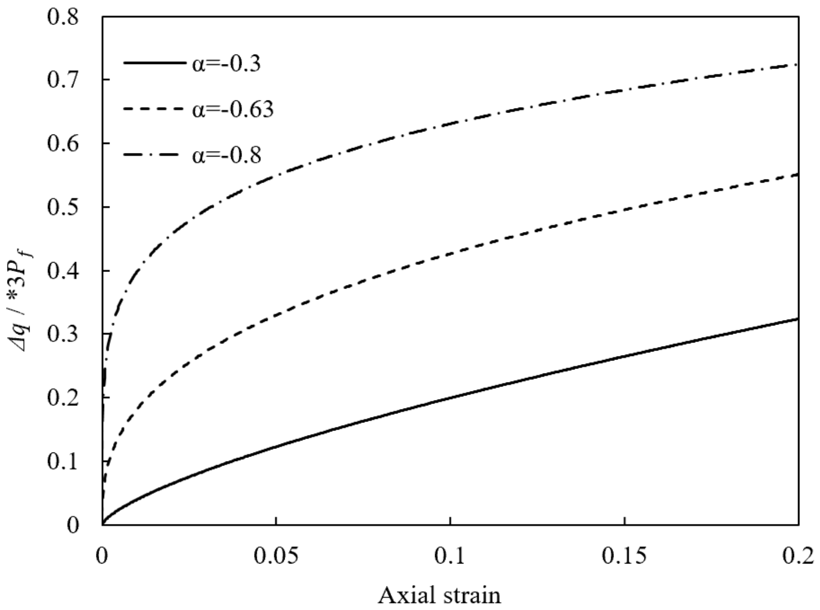
α=-0.3
α=-0.63
α=-0.8
Δq / *3P_f
Axial strain
0
0.1
0.2
0.3
0.4
0.5
0.6
0.7
0.8
0
0.05
0.1
0.15
0.2

Figure 9

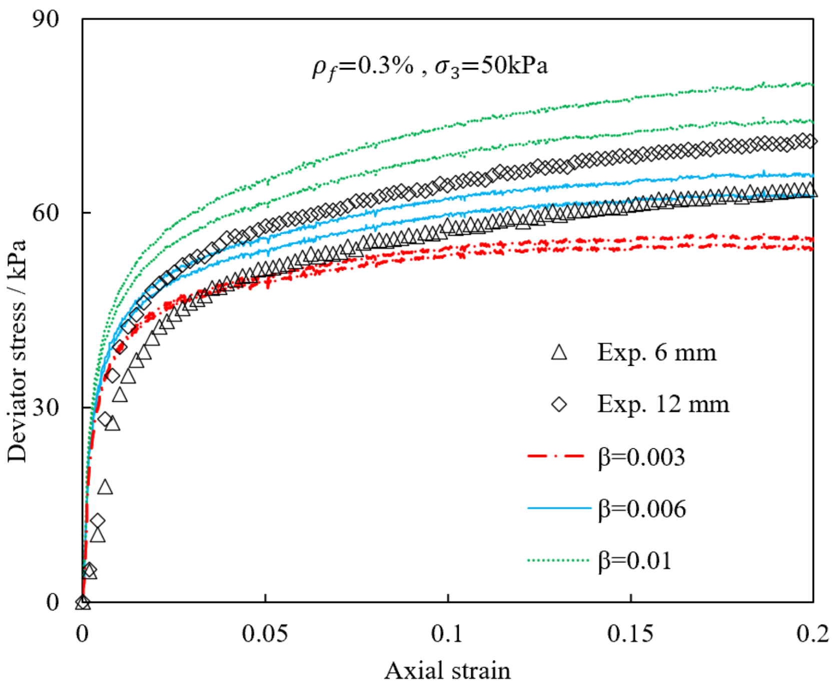
ρ_f=0.3% , σ_3=50kPa
Exp. 6 mm
Exp. 12 mm
β=0.003
β=0.006
β=0.01
Deviator stress / kPa
Axial strain
0
30
60
90
0
0.05
0.1
0.15
0.2

Figure 10

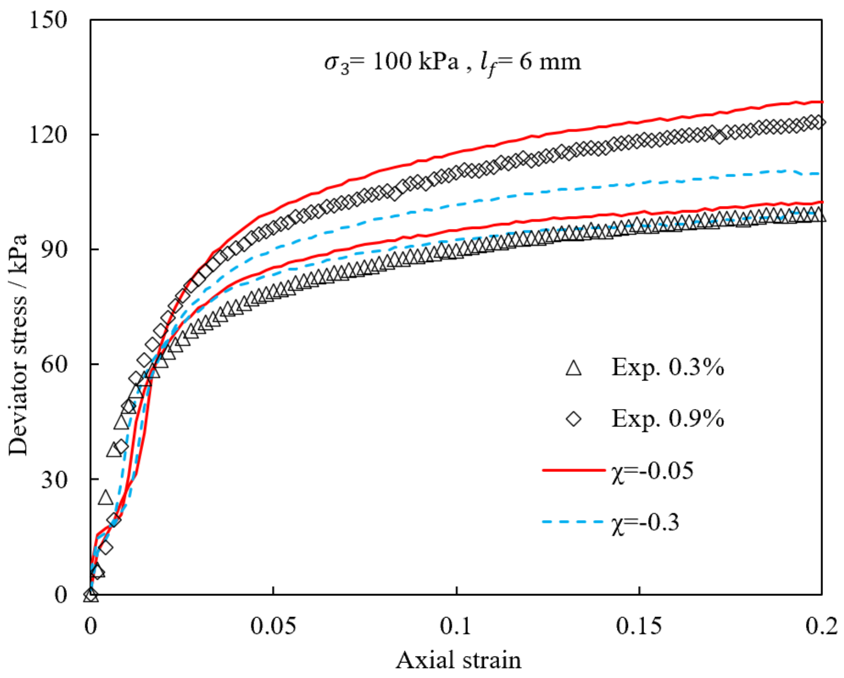

Figure 11

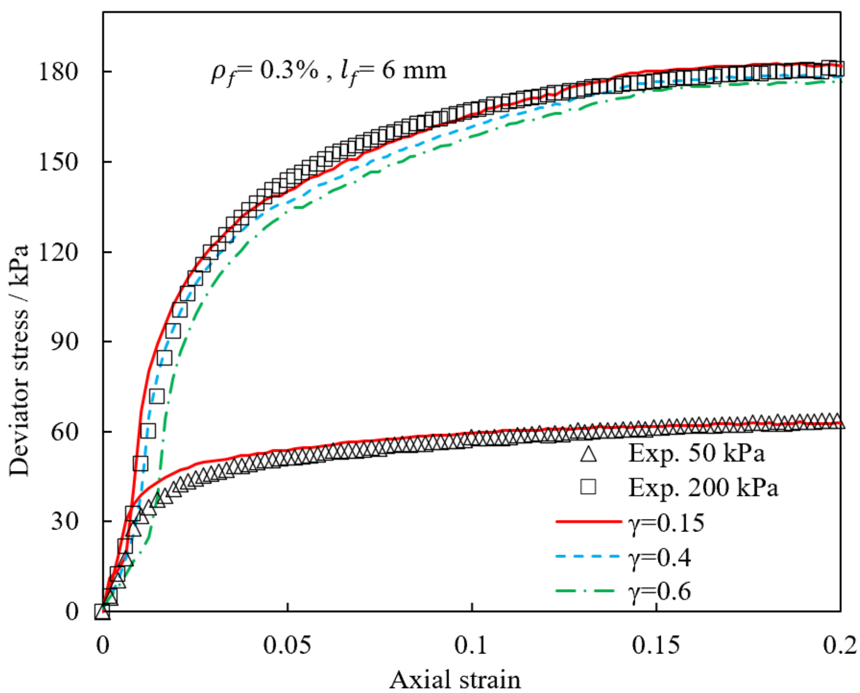

Figure 12 (a) and (b)

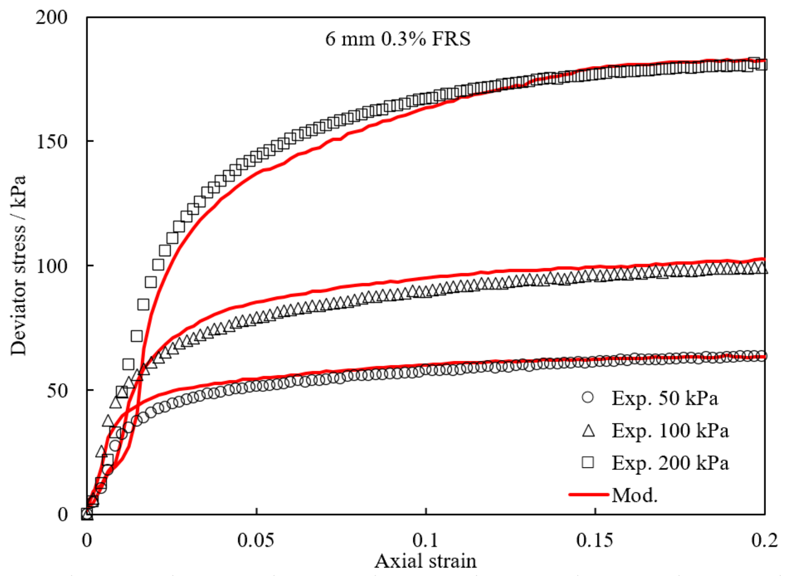

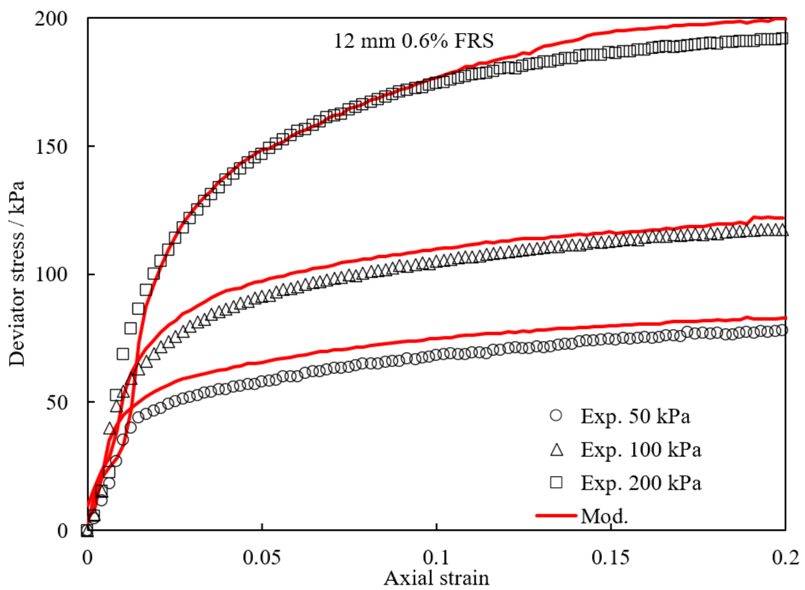

Figure 13 (a) and (b)

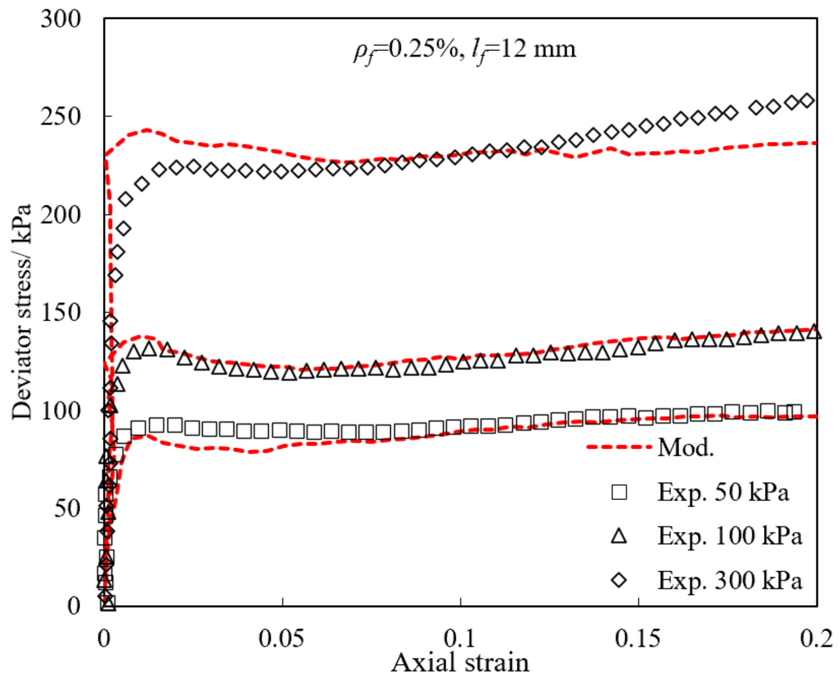

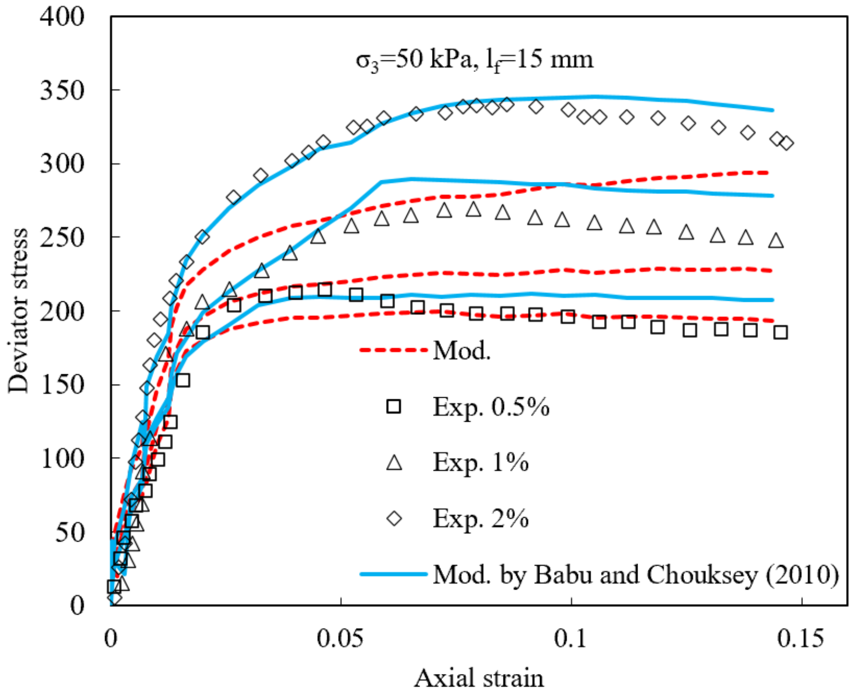

Figure 14 (a) and (b)

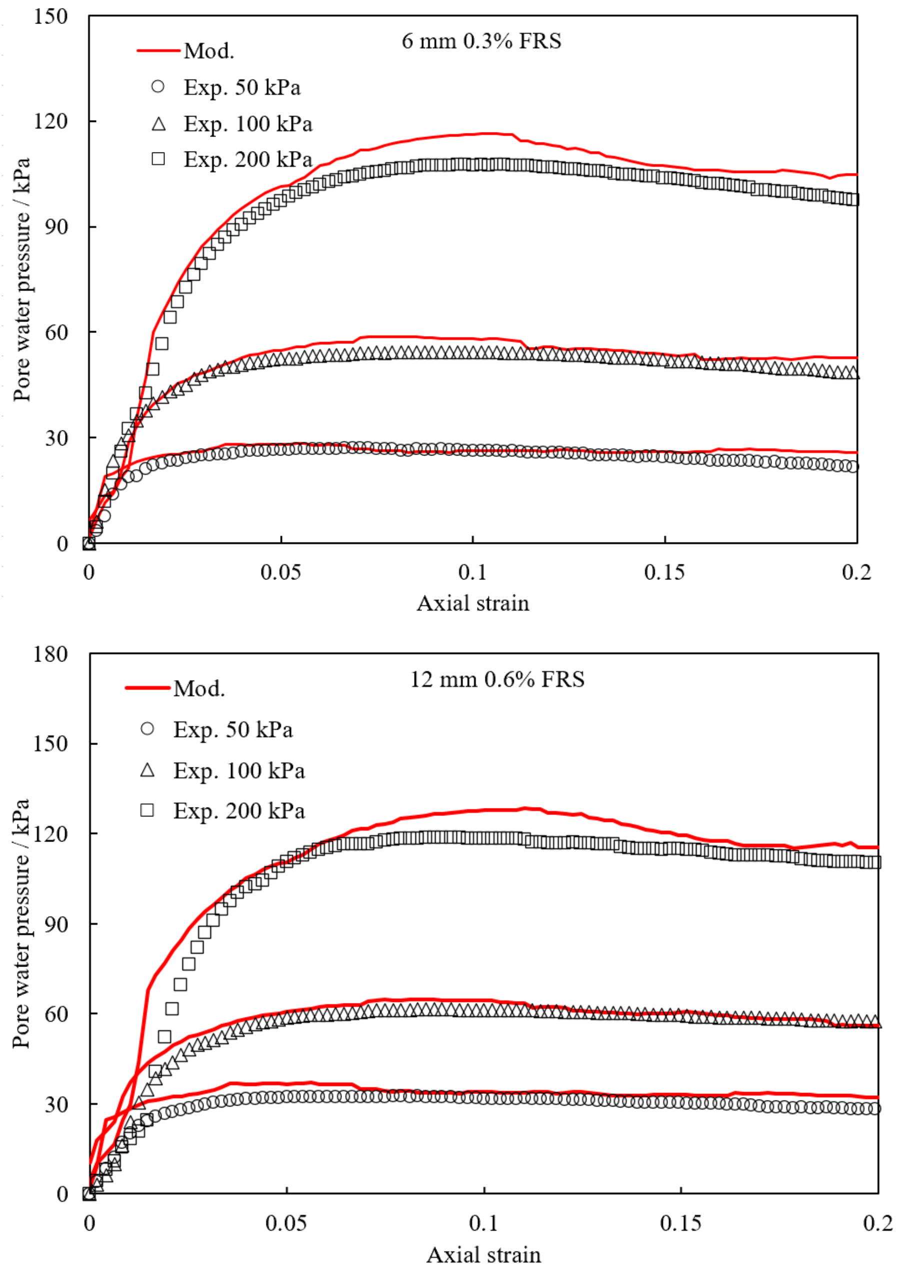
6 mm 0.3% FRS
Mod.
Exp. 50 kPa
Exp. 100 kPa
Exp. 200 kPa
Pore water pressure / kPa
Axial strain
0
30
60
90
120
150
0
0.05
0.1
0.15
0.2
12 mm 0.6% FRS
Mod.
Exp. 50 kPa
Exp. 100 kPa
Exp. 200 kPa
Pore water pressure / kPa
Axial strain
0
30
60
90
120
150
180
0
0.05
0.1
0.15
0.2

Figure 15

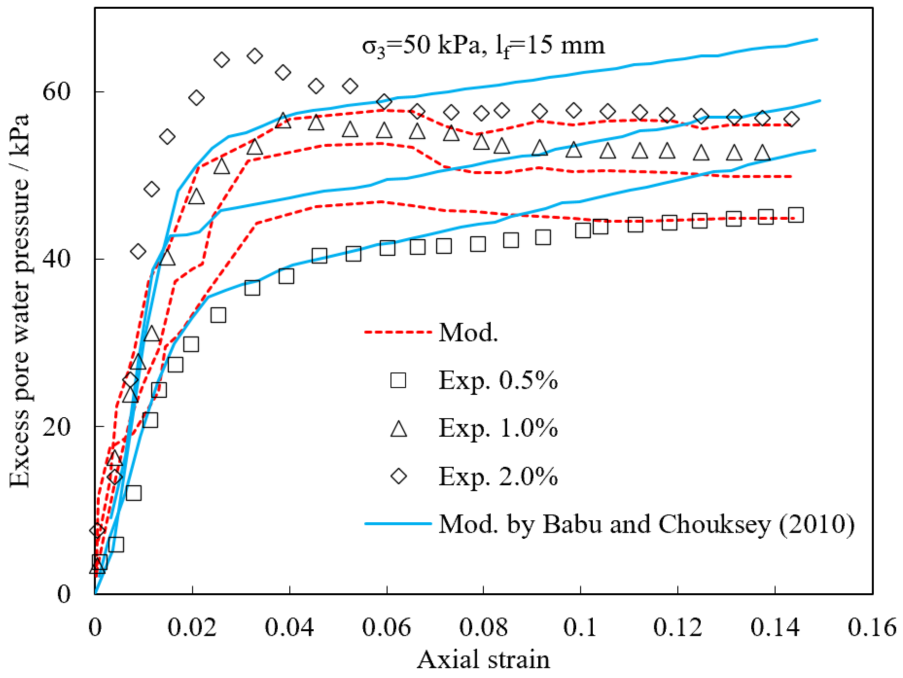

List of figure captions:

Figure 1. Appearance of polypropylene fibres used in the study.

Figure 2. Deviator stress-strain relationships of selected fibre reinforced specimens with different (a) fibre inclusion ratios (b) fibre inclusion ratios, fibre lengths and confining pressures.

Figure 3. Variations of deviator stress increment of fibre reinforced soil with different fibre inclusion ratios at 50 kPa confining pressure.

Figure 4. Normalised stress-strain curves of selected reinforced samples (l_f= 6 mm, ρ_f= 0.9%).

Figure 5. Pore water pressure-strain relationships of selected fibre reinforced specimens with different (a) fibre inclusion ratio (b) fibre inclusion ratio, fibre length and confining pressure.

Figure 6. Stress paths in p'-q plane of unreinforced soil and selected fibre reinforced soil (l_f= 6 mm, ρ_f= 0.9%) at different confining pressures.

Figure 7. Transformation of randomly distributed fibres: (a) fibres in the specimen (b) reassembled fibres (c) integration space of spherical coordinates.

Figure 8. Variation of strength improvement trend with change of sliding parameter α.

Figure 9. Influence of fibre length parameter β on the predicted results.

Figure 10. Influence of confining pressure parameter γ on the predicted results.

Figure 11. Influence of fibre inclusion ratio parameter χ on the predicted results.

Figure 12. Predicted and experimental results of stress-strain relationships of fibre reinforced clay in this study with (a) l_f= 6 mm, ρ_f= 0.3% (b) l_f= 12 mm, ρ_f= 0.6%.

Figure 13. Predicted results via the proposed model and experimental results of stress-strain relationships in (a) Corriea et al. (2021) (b) Babu and Chouksey (2010).

Figure 14. Predicted and experimental results of excess pore water pressure-strain relationship of fibre reinforced clay in this study with (a) l_f= 6 mm, ρ_f= 0.3% (b) l_f= 12 mm, ρ_f= 0.6%.

Figure 15. Predicted results via the proposed model and experimental results of excess pore water pressure-strain relationships in Corriea et al.(2021).